The effects of object activity distribution on multiplexing multi-pinhole SPECT

Greta S P Mok[1,5], **Benjamin M W Tsui**[2], and **Freek J Beekman**[3,4]

[1]Department of Electrical and Electronics Engineering, Faculty of Science and Technology, University of Macau, Taipa, Macau, People's Republic of China [2]Division of Medical Imaging Physics, Department of Radiology, Johns Hopkins Medical Institutions, Baltimore, MD 21287, USA [3]Section Radiation Detection and Medical Imaging, Faculty of Applied Sciences, Delft University of Technology, 2629JB Delft, The Netherlands [4]MILabs, Heidelberglaan 100, Utrecht, The Netherlands

Abstract

We aim to study the effects of activity distribution for multiplexing multi-pinhole (MPH) SPECT. Three digital phantoms, including a hot rod, a cold rod and a cold sphere phantom, were used. Different degrees of multiplexing were obtained by (i) adjusting the MPH pattern for the same 4-pinhole collimator (scheme 1) and (ii) increasing the number of pinholes (scheme 2). Noise-free and noisy projections were generated using a 3D analytical MPH projector based on the same acquisition time. Projections were reconstructed using OS–EM without resolution recovery. Normalized mean-square-error (NMSE), noise, image profiles and signal-to-background ratios (SBR) were assessed. For the hot rod phantom, the NMSE-noise trade-offs slightly improves for multiplexing designs in scheme 2. Substantial artifacts were observed and the NMSE-noise trade-offs slightly worsened for multiplexing designs for the cold phantoms. Resolutions slightly degraded for higher degrees of multiplexing (~39–65%) for the cold rod phantom. For the cold sphere phantom, image profiles showed non-multiplexing designs better emulated the phantom, while ~20% multiplexing performs similarly as compared to non-multiplexing in SBR. Our results indicate that multiplexing can help for sparse objects but leads to a significant image degradation in non-sparse distributions. Since many tracers are not highly specific, and the gain of detection efficiency by allowing multiplexing is fairly offset by image degradations, multiplexing needs to be kept to a minimum for optimum MPH collimator designs.

Introduction

Conventional SPECT using a parallel-hole collimator lacks sufficient detection efficiency and resolution trade-off for imaging small animals such as rodents, especially their even smaller organs-of-interest. High-resolution SPECT using a pinhole collimator, especially the multi-pinhole (MPH) collimator, with an appropriate pinhole pattern arrangement, has been recognized to provide improved image quality as compared to that by conventional parallel-hole and single pinhole (SPH) collimators, anchoring its unique role for the molecular imaging of small animals (Beekman and Van der Have 2007, Jaszczak *et al* 1994, Meikle *et al* 2005, Nuyts *et al* 2009, Freed *et al* 2008, Metzler *et al* 2005, Strand *et al* 1994, DiFilippo 2008). Multiple research and commercial systems with different design parameters are now available (Van der Have *et al* 2009, Schramm *et al* 2003, Kim *et al* 2006, Lackas *et al* 2005,

DiFilippo 2008). Although most of the design parameters, such as the number and placement of pinholes, collimator length, aperture size and degree of multiplexing, i.e. projection overlapping from neighboring apertures, have been studied, there is still no consensus about the optimized MPH design as it always depends on the detector size, intrinsic resolution and, ultimately, the specific application with specific object activity distribution.

Among all MPH SPECT system design parameters, multiplexing is the one that draws a lot of attention. Justifications that are being used for multiplexing in the projections, as once studied by the authors (Mok *et al* 2009), are to further increase detection efficiency by having a larger number of pinholes or allowing a shorter radius-of-rotation (ROR), or to improve spatial resolution by having a larger magnification factor (figure 1). However, studies have demonstrated that multiplexing poses ambiguous information for reconstructions which may lead to non-unique solutions for the inverse problem, because counts in the overlapping region cannot be traced back through a particular pinhole aperture (Vunckx *et al* 2008, Mok *et al* 2009) and significant longer image reconstruction times are needed to suppress multiplexing artifacts. These substantial adverse effects are actually intertwined with the pinhole pattern and are more prominent for certain non-optimized pinhole patterns (Mok *et al* 2005).

Vunckx *et al* (2008) studied the effect of overlapping projections based on simulations with homogeneous sphere and rat brain phantoms. They conclude that once the detector area has been fully utilized, the extra detection efficiency can only compensate for the ambiguity posed by multiplexing, and removing overlap actually improves the contrast-to-noise ratio especially for the central field-of-view. Results from Mahmood *et al* (2010) also showed that multiplexing leads to image artifacts as compared to non-multiplexing designs; however, they found that spatial resolution can be maintained and noise can be reduced for high degrees of multiplexing given that non-multiplexed data were also incorporated into the reconstructions. The authors also showed that improved detection efficiency and resolution by increased multiplexing are offset by increased image NMSE (Mok *et al* 2009), and the common belief is that the tolerance for multiplexing depends on the specific imaging task.

The extreme case for multiplexing is coded aperture collimation with lots of pinholes (~100). It was originally proposed and works well for far-field applications, such as high-energy astronomical imaging with bright and isolated sources (Caroli *et al* 1987). Accorsi *et al* (2001) validated the relationship between SNR improvement and sensitivity gain with a coded aperture for point sources, and demonstrated its usage in imaging high contrast point-like objects with ^{125}I tracer when coupled to a hybrid pixel detector (Accorsi *et al* 2008). However, the majority of tracers for nuclear medicine imaging do not bind to the targets with high specificity, and as a result background activity always exists. The common diagnostic tasks in SPECT include detecting hot lesions, cold defects and quantifying tracer concentrations, and multiplexing may have a different impact on each of these application areas. This leads to the question `Is the effect of multiplexing dependent on the specific tracer distributions?' which was briefly discussed by Vunckx *et al* for two different phantoms (Vunckx *et al* 2008). This study aims to address this concern with simulations using hot and cold rod digitized phantoms and a digitized cold sphere phantom.

Materials and methods

Simulation setup

We simulated a `focusing' MPH projection configuration, i.e. all pinhole axes are focusing on the center of the object. Three different digitized phantoms with the same outer diameter and length of 24 mm were used in the simulation: (i) a hot rod phantom (figure 2(a)); (ii) a

cold rod phantom (figures 2(b)) and (iii) a cylindrical cold sphere phantom where a 4.2 mm sphere with signal-to-background-ratio (SBR) of 0.3 was placed at the center of a uniform cylinder (figure 2(c)). The rod phantoms were used to assess the possible resolution loss due to multiplexing, while the cold sphere phantom, mimicking a cold lesion on a uniform background, was used to investigate possible artifacts. Similar phantoms are used for testing clinical and preclinical SPECT systems. Using a 3D MPH analytical projector, we modeled a MPH SPECT system with a single detector with a size of 12×12 cm and an intrinsic resolution of 1.5 mm. The simulated projection matrix size was 0.1 mm and the reconstructed voxel size was 0.3 mm in order to mimic the continuous character of tracer distributions. We simulated 64 projections over 360° with one bed position. The analytical simulation tool was implemented in C based on a Unix platform, and the system matrix was computed using a pixel driven projector and backprojector, with modeling of resolution and detection efficiency based on theoretical derivations (Wang 2004). Noise-free and ensembles of noisy projection data with 20 noise realizations were generated by adding Poisson noise to the noise-free projections for each phantom and experimental set up. The noise level represented an acqusition time of 10 mins and an activity of 0.5 mCi, 2.4 mCi and 3 mCi for the hot rod phantom, cold rod phantom and cold sphere phantom, respectively.

We reconstructed the projection data with up to 240 updates using an iterative OS–EM based 3D MPH reconstruction algorithm with eight subsets while resolution recovery was not used (Wang and Tsui 2007). Penetration, attenuation and scatter in the collimator-detector, attenuation and scatter in the objects are not modeled in the projector and reconstruction method.

Multiplexing schemes

We obtained four different degrees of multiplexing for each phantom by setting up the imaging geometry differently. The overlapping regions of the projection were identified on the projection images, and the degree of multiplexing was defined in the projection/detector space as (figure 3)

$$\%\text{multiplexing}=\frac{\text{number of pixel with multiplexing in each angular view}}{\text{number of pixel with non}-\text{zero value in each angular view}}.$$

Multiplexing scheme 1: fixed number of pinholes—We simulated a 4-pinhole configuration and obtained 4 degrees of multiplexing for different phantoms in the projections by changing the scaling of the pinhole pattern as the positions of the pinhole apertures were moved gradually closer to each other (figure 3(a)). Simulations for different settings were based on the same ROR and magnification.

Multiplexing scheme 2: variable number of pinholes—We considered 4 degrees of multiplexing for different phantoms in the projections by solely increasing the number of pinholes (figure 3(b)). We simulated 4-, 5-, 7- and 9-pinhole configurations and simulations for different settings were based on the same ROR and magnification.

The multiplexing scheme 1 was designed to study the multiplexing effect independently, without intertwining with the effects from other confounding factors such as resolution and detection efficiency. The multiplexing scheme 2 where the whole detector space was fully utilized represents a more common design approach, i.e. to improve the detection efficiency with more pinholes where all pinholes were placed in different axial planes to improve axial sampling as shown in figure 4(a).

A summary for the system configuration parameters employed in this work is listed in table 1 and the imaging geometry is shown in figure 4. The details about the parameters used in the aforementioned simulation studies are listed in table 2.

Data analysis

Besides visual assessment to identify artifacts, we used the normalized-mean-square-error (NMSE) between the whole 3D noisy reconstructed images and the original phantoms to study possible artifact generations due to multiplexing for all phantoms:

$$\text{average NMSE} = \frac{1}{n} \sum_{j=1}^{n} \left(\frac{x_j - \lambda_j}{\bar{\lambda}} \right)^2. \tag{1}$$

n: number of voxels in the whole reconstructed volume.

γ: voxel count value in the original phantom.

$\bar{\lambda}$: mean voxel value of the original phantom.

x: voxel count value in the noisy reconstructed image.

j: voxel index.

The normalized standard deviation (NSD) image, used as the noise index, was calculated based on the mean and variance reconstructed images obtained from the 20 noisy projection realizations. We then computed the mean value of the NSD in a 3D uniform region with 1,800 voxels, visually chosen in the reconstructed image to avoid artifacts:

$$\text{average NSD} = \frac{1}{n} \sum_{j=1}^{n} \frac{\sqrt{\frac{1}{m-1} \Sigma_{i=1}^{m} \left(x_j^i - \bar{x}_j \right)^2}}{\bar{x}_j}. \tag{2}$$

m: number of noise realizations.

n: number of voxels in the selected uniform region in the reconstructed image.

x: voxel count value in the noisy reconstructed image.

$\bar{x}$: voxel count value in the mean reconstructed image.

i: noise realization index.

j: voxel index.

The 3D signal-to-background ratio (SBR) was calculated from the chosen signal and background regions for different degrees of multiplexing and updates of the noisy reconstructed images as shown in figure 5, in the cold sphere phantom simulation:

$$\text{SBR} = \frac{\text{Mean } cold\ sphere}{\text{Mean } background}. \tag{3}$$

The SBR was used as a quantitative figures-of-merit to study contrast in the noisy reconstructed images, while image profiles were taken in the uniform region from the noise-free reconstructed images to study uniformity. The trade-off between NMSE and noise in

the reconstructed images is also assessed for different multiplexing schemes and activity distributions.

Results

From visual assessment, generally, no significant `ghost artifacts' were observed in the reconstructed images, illustrating the appropriate choice of the pinhole patterns. In the following we discuss some specific findings for each phantom simulation experiment.

Hot rod phantom

The image degradations are least significant for the hot rod phantom as compared to other phantoms. From visual assessment, there are no significant resolution degradations for both noise-free and noisy reconstruction images. In both multiplexing schemes, the 1.2 mm hot rods can be visualized for all degrees of multiplexing for the noise free images while the 1.6 mm hot rods can be observed for all degrees of multiplexing in the noisy images (figures 6(a) and (b)). The NMSE, calculated from the noisy reconstructed images, reduces slightly for the non-multiplexing design as compared to the multiplexing designs for scheme 1 and vice versa for scheme 2 (figures 6(c)–(f)), NMSE to noise trade-off curves show that a higher degree of multiplexing actually performs slightly better than a non-multiplexing design in scheme 2. Their difference is generally very subtle and not significant for both schemes (figures 6(g) and (h)).

Cold rod phantom

Noticeable image degradations are observed for the cold rod phantom as compared to the hot rod phantom. From visual assessment, ring artifacts are noticeable for both noise free and noisy reconstructions for higher degrees (~39% to ~65%) of multiplexing under both schemes (figures 7(a) and (b)). Resolutions are slightly degraded for higher degrees of multiplexing, as the contrast of the smallest observable cold rods, i.e. 1.2 and 1.6 mm cold rods for noise free and noisy cases respectively, is worse for higher degree of multiplexing. Quantitative assessment from the noisy data sets shows that avoiding multiplexing slightly reduces NMSE for both schemes (figures 7(c)–(f)). No multiplexing provides slightly better NMSE to noise trade-off compared to designs with multiplexing for both schemes (figures 7(g) and (h)).

Cold sphere phantom

The image degradations due to multiplexing are more apparent for the cold sphere phantom than for the others. From a visual assessment, both coronal and transaxial images show artifacts for both noise-free and noisy reconstructions with increased projection multiplexing under both schemes (figures 8(a) and (b), arrows). Quantitative measurements from the noisy data show that for both schemes, avoiding multiplexing reduces NMSE more significantly as compared to other phantoms (figures 8(c)–(f)). Corresponding NMSE-to-noise trade-off curves show that the non-multiplexing design offers better image quality than that of the multiplexing designs and their differences are most obvious for scheme 1 (figures 8(g) and (h)), which may be attributed to the artifacts generated for this specific activity distribution combined with the multiplexing patterns. Due to the specific overlapping pattern of the projections, higher or lower intensity ring and band artifacts perpetuate in the reconstructed images for different degrees of multiplexing (figures 8(a) and (b), arrows), causing the underestimation of the SBR for a higher degree of multiplexing in both schemes (figures 8(i) and (j)). However, the SBR to noise trade-off of %M (multiplexing)= ~20% (red line) is similar to that of the non-multiplexing designs (blue line) in both schemes (figures 8(i) and (j)). The non-uniformity caused by multiplexing is illustrated by the image

profiles drawn across a uniform region of the cylindrical background (figures 8(k) and (l)). These profiles indicate that no multiplexing results in the least image artifacts.

Discussion

Due to the many interrelated variables involved in designing a MPH collimator, e.g. acceptance angle of the pinhole aperture, pinhole pattern, collimator length, pinhole number, degree of multiplexing, aperture size, detector size and imaging distance, there is no consensus on an optimal MPH collimator design, which is task dependent (Cao *et al* 2005, Bal *et al* 2004). In this simulation study, we focused on investigating the correlations between object activity distributions and multiplexing on the reconstruction image quality by using three digitized phantoms with different activity distributions.

Noise-free reconstructed images for all phantoms offer an evident visualization of the effects of multiplexing on artifacts generations on the reconstructed images. While resolution degradations are not significant for the hot rod phantom for all degrees of multiplexing, they are apparent for the cold rod phantom for higher degrees of multiplexing. From both qualitative and quantitative measurements, artifacts are most apparent for the cold sphere phantom for higher degrees of multiplexing, while artifacts in the cold rod phantom are a bit more significant than in the hot rod phantom. The lack of background activity distribution may contribute to the slight advantage for multiplexing in the hot rod phantom, similar to the use of coded aperture for the astronomical applications. Although the appearance, position and intensity of the artifacts are dependent on the degree of multiplexing and specific activity distribution, ring artifacts dominate especially in the uniform region and artifacts generally perpetuate over the whole reconstructed object as illustrated by the quantitative NMSE-noise trade-offs and image profile measurements in the cold sphere phantom. Thus, while multiplexing may not pose a significant problem for detection of a substantial lesion, the quantitative accuracy is inevitably affected for MPH designs with multiplexing. Our results are in concordance with the findings from Vunckx *et al* (2008) and Mahmood *et al* (2010) that excessive multiplexing generally induces artifacts and gains of multiplexing are actually offset by the associated image degradations.

While Vunckx *et al* (2008) computed multiplexing based on the reconstructed voxels, the definition of multiplexing in this paper and that from Mahmood *et al* are based on the projection which is more intuitive (Mahmood *et al* 2010, Mok *et al* 2009) and results from all these studies are in accordance. The main justification used for promoting multiplexing is to increase detection efficiency. The NMSE-noise trade-off results from scheme 2 show that gain of detection efficiency from multiplexing is actually evenly offset by the image degradations for the cold rod phantoms. The gain is even over-offset from the image degradations for the cold sphere phantom. The difference between the two schemes is generally in accordance. For the SBR-to-noise trade-offs, the SBR deviates more from the truth for a higher degree of multiplexing of ~40% for both schemes. This may be due to the dark and bright band artifacts generated from the specific overlapping patterns, which may create an artifactual decrease in SBR as compared to the truth, and the high and low intensity artifacts due to multiplexing tends to cancel out each other for multiplexing of ~60% in scheme 2.

The NMSE-to-noise and SBR-to-noise trade-off results measured from the noisy data indicate a region for optimal image quality, i.e. the bottom left corner when noise and NMSE are low. Thus, a higher numbers of updates are not necessary in this case though one may argue that artifacts may reduce for a higher number of updates. However, studies from Mahmood *et al* (2010) also showed that the artifacts persist even after more than 1,636 updates in noise free situations.

The common concept for multiplexing is that the reconstruction algorithm is less susceptible in generating artifacts for a more focused or a centrally concentrated activity distribution. However, in preclinical and clinical imaging where an extended background always exists, this understanding may not be necessarily right. The results from the three phantoms in this study show the general consensus that the image degradations of multiplexing offset is associated gain of detection efficiency for the non-sparse phantoms, though it may pose some advantages for the sparse distributions such as the hot rod phantom. Thus, an increasing number of pinholes with the associated increase of multiplexing leads to an inferior MPH collimator design, i.e. with substantial image artifacts and a longer reconstruction time for general nuclear medicine imaging. Other researchers used other phantoms representing more realistic clinical situations, i.e. a Hoffman brain phantom, a Zubal phantom simulating a dopamine receptor study and a rat brain phantom (Mahmood *et al* 2010). Their results are also similar to our investigation, indicating that although the extent of artifacts caused by multiplexing may slightly vary for different activity distributions, its degradation on image quality or quantitative accuracy inevitably exists for general nuclear medicine applications. Suggestions made by the researchers for alleviating the multiplexing artifacts include complete blockage of overlapping using physical septa (Vunckx *et al* 2008, Beekman *et al* 2005, Van der Have *et al* 2009), and mixing the multiplexing data with non-multiplexing data for reconstructions (Mahmood *et al* 2010), which shows promising results in artifact reduction. Another solution is to acquire projections at a number of imaging distances, known as synthetic collimator, so that the amount of multiplexing varies and provides more information for reconstruction (Wilson *et al* 2000, Shokouhi *et al* 2009).

Another potential advantage for allowing multiplexing is reducing the projection truncation which may lead to reconstructed artifacts (figure 9), as the object of interest is very likely not being fully covered in the field-of-view for every pinhole and every projection view in non-multiplexing design. In some cases this situation leads to an interior problem and may hamper a correct reconstruction, although corrections for this problem are proposed, e.g. shifting the object during the projection acquisition (Van der Have *et al* 2009) or adding *a priori* knowledge (Kudo *et al* 2007). The pinhole design with a bigger acceptance angle and a more titled pinhole axis may be at the cost of more edge penetration. Wang and Tsui (2006) studied the trade-off between truncation and multiplexing based on the crosstalk concept and claimed that combination of truncation and multiplexing posed an even more adverse effect in image reconstruction. We tried to avoid truncation for most experimental designs, for example, by having a larger acceptance angle, bigger ROR and shorter phantom in this study as this research topic needs a further independent investigation.

There are certain limitations in this study. The simulations are based on a small gamma camera with relatively high intrinsic resolution and low magnification factor. Though the phantom size is similar to mouse imaging, the ROR used, i.e. 4 cm, resembles more of a rat-imaging situation, in order to avoid truncation. For the same reason, the length of the phantom used is also shorter than that of a realistic animal. The order of multiplexing was not explored in this study and its effect on reconstructed image quality needs further investigation. Also, resolution recovery and other physical image degradations such as penetration, attenuation and scatter are not used in this study. Further investigations are needed for more realistic or advanced pinhole SPECT systems, e.g., (i) systems that allow 3D targeting imaging using an XYZ stage (Van der Have *et al* 2009, Branderhorst *et al* 2011), (ii) systems that employ better system resolution models in reconstruction algorithms such as OS-EM, COSEM or POSEM (Branderhorst *et al* 2010), or (iii) systems with projection truncation.

Conclusions

We have studied the effects of activity distribution on multiplexing in terms of image profiles, NMSE-noise and contrast-noise trade-offs in the reconstructed images. Our results suggest that the gains in detection efficiency from increased multiplexing are offset by increased image degradation in terms of NMSE and noise especially for a cold rod phantom and a cold sphere phantom. The artifacts seem to be insignificant for the hot rod phantom with no background distribution while they are clearly noticeable for the cold rod and even more severe for the cold sphere phantom. Also with multiplexing, more iterations are needed to converge to acceptable images, which was also found in earlier experiments by Meikle *et al* (2002). The quantitative measures show that excessive multiplexing worsens the image quality for the cold phantoms for a compact gamma camera with size of 12×12 cm. Generally, multiplexing degrades image quality for non-sparse phantoms and should be kept to a minimum in MPH collimator designs, although the correlation between truncation and multiplexing is still not fully explored and may shed new light on present and future design concepts. In addition, results may differ for systems with other pinhole geometries such as targeting system or those with truncated projections that may be even more sensitive to multiplexing induced artifacts.

Acknowledgments

References

Accorsi R, Celentano L, Laccetti P, Lanza RC, Marotta M, Mettivier G, Montesi MC, Roberti G, Russo P. High-resolution I-125 small animal imaging with a coded aperture and a hybrid pixel detector. IEEE Trans. Nucl. Sci. 2008; 55:481–90.

Accorsi R, Gasparini F, Lanza RC. A coded aperture for high-resolution nuclear medicine planar imaging with a conventional anger camera: Experimental results. IEEE Trans. Nucl. Sci. 2001; 48:2411–7.

Bal G, Zeng GL, Lewitt RM, Cao Z, Acton PD. Study of different pinhole configurations for small animal tumor imaging. 2004 IEEE Nuclear Science Symp. Conf. Record. 2004; 1–7:3133–7.

Beekman F, Van Der Have F. The pinhole: gateway to ultra-high-resolution three-dimensional radionuclide imaging. Eur. J. Nucl. Med. Mol. Imaging. 2007; 34:151–61. [PubMed: 17143647]

Beekman FJ, Van Der Have F, Vastenhouw B, Van Der Linden AJA, van Rijk PP, Burbach JPH, Smidt MP. U-SPECT-I: a novel system for submillimeter-resolution tomography with radiolabeled molecules in mice. J. Nucl. Med. 2005; 46:1194–200. [PubMed: 16000289]

Branderhorst W, Vastenhouw B, Beekman F. Pixel-based subsets for rapid multi-pinhole SPECT reconstruction. Phys. Med. Biol. 2010; 55:2023–34. [PubMed: 20299722]

Branderhorst W, Vastenhouw B, Van Der Have F, Blezer E, Beekman FJ. Targeted multi-pinhole SPECT. Eur. J. Nucl. Med. Mol. Imaging. 2011; 38:552–61. [PubMed: 21063706]

Cao Z, Bal G, Accorsi R, Acton PD. Optimal number of pinholes in multi-pinhole SPECT for mouse brain imaging—a simulation study. Phys. Med. Biol. 2005; 50:4609–24. [PubMed: 16177493]

Caroli E, Stephen JB, Dicocco G, Natalucci L, Spizzichino A. Coded aperture imaging in x-ray and gamma-ray astronomy. Space Sci. Rev. 1987; 45:349–403.

DiFilippo FP. Design and performance of a multi-pinhole collimation device for small animal imaging with clinical SPECT and SPECT-CT scanners. Phys. Med. Biol. 2008; 53:4185–201. [PubMed: 18635899]

Freed M, Kupinski MA, Furenlid LR, Wilson DW, Barrett HH. A prototype instrument for single pinhole small animal adaptive SPECT imaging. Med. Phys. 2008; 35:1912–25. [PubMed: 18561667]

Jaszczak RJ, Li JY, Wang HL, Zalutsky MR, Coleman RE. Pinhole collimation for ultra-high-resolution, small-field-of-view spect. Phys. Med. Biol. 1994; 39:425–37. [PubMed: 15551591]

Kim H, Furenlid LR, Crawford MJ, Wilson DW, Barber HB, Peterson TE, Hunter WCJ, Liu ZL, Woolfenden JM, Barrett HH. SemiSPECT: a small-animal single-photon emission computed tomography (SPECT) imager based on eight cadmium zinc telluride (CZT) detector arrays. Med. Phys. 2006; 33:465–74. [PubMed: 16532954]

Kudo H, Courdurier M, Noo F, Defrise M. Tiny a priori knowledge solves the interior problem. 2007 IEEE Nuclear Science Symp. Conf. Record. 2007; 1–11:4068–75.

Lackas C, Schramm NU, Hoppin JW, Engeland U, Wirrwar A, Halling H. T-SPECT: a novel imaging technique for small animal research. IEEE Trans. Nucl. Sci. 2005; 52:181–7.

Mahmood ST, Erlandsson K, Cullum I, Hutton BF. The potential for mixed multiplexed and non-multiplexed data to improve the reconstruction quality of a multi-slit-slat collimator SPECT system. Phys. Med. Biol. 2010; 55:2247–68. [PubMed: 20354282]

Meikle SR, Kench P, Kassiou M, Banati RB. Small animal SPECT and its place in the matrix of molecular imaging technologies. Phys. Med. Biol. 2005; 50:R45–61. [PubMed: 16264248]

Meikle SR, Kench P, Weisenberger AG, Wojcik R, Smith MF, Majewski S, Eberl S, Fulton RR, Rosenfeld AB, Fulham MJ. A prototype coded aperture detector for small animal SPECT. 2001 IEEE Nuclear Science Symp., Conf. Records. 2002; 1–4:1580–4.

Metzler SD, Jaszczak RJ, Patil NH, Vemulapalli S, Akabani G, Chin BB. Molecular imaging of small animals with a triple-head SPECT system using pinhole collimation. IEEE Trans. Med. Imaging. 2005; 24:853–62. [PubMed: 16011314]

Mok, GS.; Tsui, BM.; Wang, Y.; Du, Y.; Segars, WP.; Frey, EC. Effects of pinhole pattern and multiplexing in multi-pinhole small animal SPECT. 52nd Annu. Meeting of the Society of Nuclear Medicine; Toronto, Canada. 2005.

Mok GS, Wang Y, Tsui BM. Quantification of the multiplexing effects in multi-pinhole small animal SPECT—a simulation study. IEEE Trans. Nucl. Sci. 2009; 56:2636–43.

Nuyts J, Vunckx K, Defrise M, Vanhove C. Small animal imaging with multi-pinhole SPECT. Methods. 2009; 48:83–91. [PubMed: 19328232]

Schramm NU, Ebel G, Engeland U, Schurrat T, Behe M, Behr TM. High-resolution SPECT using multipinhole collimation. IEEE Trans. Nucl. Sci. 2003; 50:315–20.

Shokouhi S, Metzler SD, Wilson DW, Peterson TE. Multi-pinhole collimator design for small-object imaging with SiliSPECT: a high-resolution SPECT. Phys. Med. Biol. 2009; 54:207–25. [PubMed: 19088387]

Strand SE, Ivanovic M, Erlandsson K, Franceschi D, Button T, Sjogren K, Weber DA. Small animal imaging with pinhole single-photon emission computed-tomography. Cancer. 1994; 73:981–4. [PubMed: 8306288]

Van Der Have F, Vastenhouw B, Ramakers RM, Branderhorst W, Krah JO, Ji CG, Staelens SG, Beekman FJ. U-SPECT-II: an ultra-high-resolution device for molecular small-animal imaging. J. Nucl. Med. 2009; 50:599–605. [PubMed: 19289425]

Vunckx K, Suetens P, Nuyts J. Effect of overlapping projections on reconstruction image quality in multipinhole SPECT. IEEE Trans. Med. Imaging. 2008; 27:972–83. [PubMed: 18599402]

Wang, Y. Department of Biomedical Engineering. The University of North Carolina; Chapel Hill: 2004. Development and application of high-sensitivity and high-resolution fully 3D SPECT imaging techniques using two different collimator designs.

Wang, Y.; Tsui, BM. IEEE Nuclear Science Symp. and Medical Imaging Conf. San Diego, USA: 2006. Application of crosstalk concept to assessment of multi-pinhole collimator designs in small animal SPECT imaging.

Wang YC, Tsui BMW. Pinhole SPECT with different data acquisition geometries: usefulness of unified projection operators in homogeneous coordinates. IEEE Trans. Med. Imaging. 2007; 26:298–308. [PubMed: 17354636]

Wilson DW, Barrett HH, Clarkson EW. Reconstruction of two- and three-dimensional images from synthetic-collimator data. IEEE Trans. Med. Imaging. 2000; 19:412–22. [PubMed: 11021685]
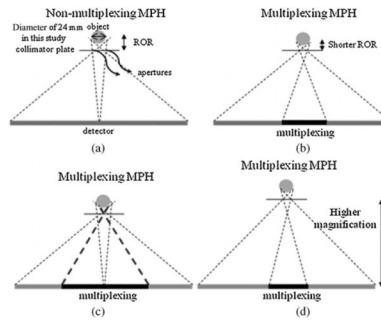
Figure 1.
When compared to a non-multiplexing MPH design (a), which shows a simplified 2-pinhole configuration here, multiplexing can improve detection efficiency by allowing a shorter ROR (b), by packing a larger number of pinholes (3 pinholes here) (c) or by increasing the magnification for improved resolution in the projection domain as each projection contains more resolvable detector pixel elements (d).
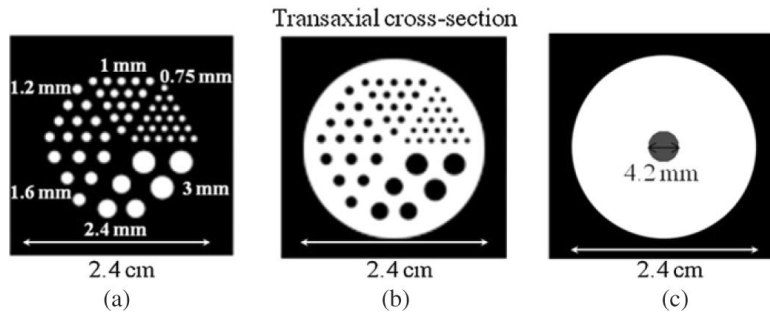
Figure 2.
The three phantoms with different activity distributions that were used in the study: (a) hot rod phantom with rod sizes ranging from 0.75 to 3 mm, (b) cold rod phantom with the same rod sizes as the hot rod phantom, and (c) cold sphere phantom with signal-to-background ratio (SBR) of 0.3.

(a)

(b)
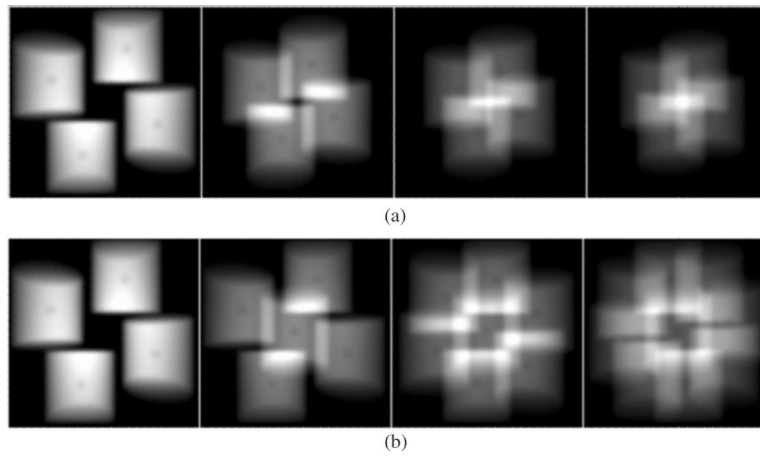
Figure 3.
Sample noise-free projection data of the cold sphere phantom are used to demonstrate the multiplexing schemes. Four degrees of multiplexing are obtained by (a) adjusting the 4-pinhole pattern (0%, 22%, 38% and 42%), and (b) increasing the pinhole number from 4- to 9-pinholes (0%, 19%, 39% and 60%) for the cold sphere phantom.
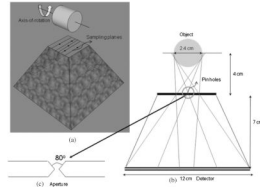
Figure 4.
The imaging geometry of the simulation set up of the 5-pinhole imaging for the cold sphere phantom shown in (a) 3D and (b) 2D. A close up view of the pinhole aperture is shown in (c).
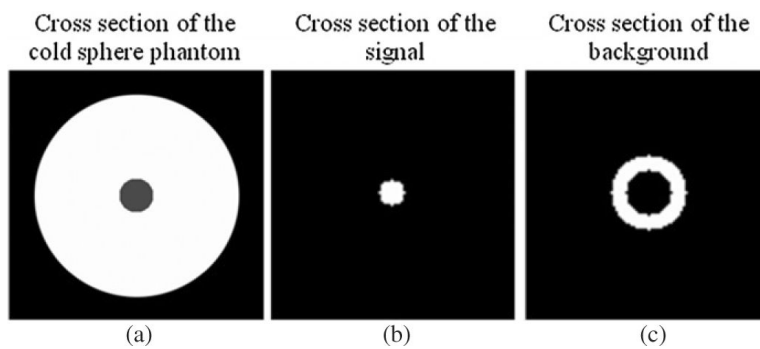
Figure 5.
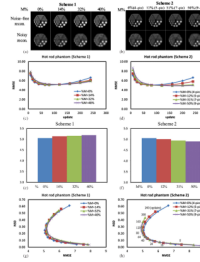(a) Original cold sphere phantom, (b) signal region and (c) background region for calculating the SBR.

Figure 6.
Samples of noise-free and noisy reconstruction images (after 120 updates) for the hot rod phantom for different degrees of multiplexing obtained from (a) scheme 1 (same number of pinholes) and from (b) scheme 2 (increasing number of pinholes). The NMSE shown as a function of number of updates for increased degrees of multiplexing for (c) scheme 1 and (d) scheme 2. (e) and (f) The lowest NMSE achieved for different degrees of multiplexing for the two schemes. (g) and (h) Corresponding NMSE-to-noise trade-off curves for different degrees of multiplexing for both schemes.
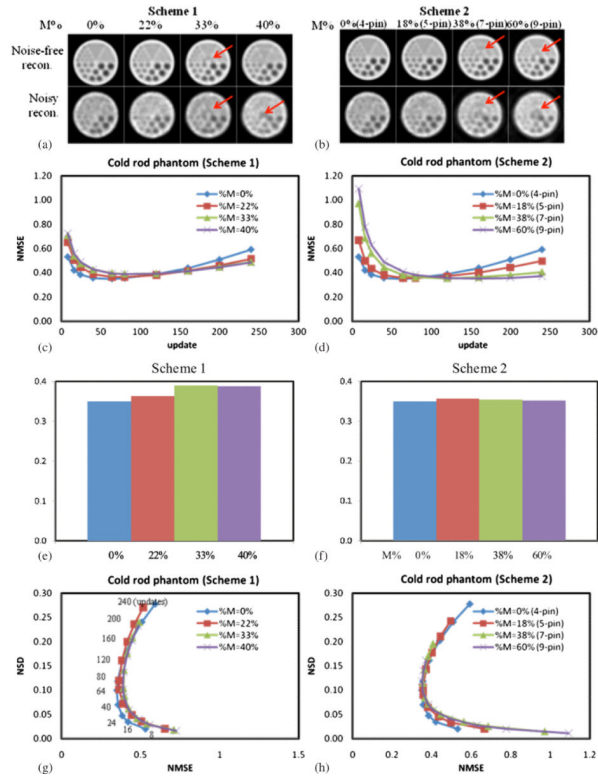
Figure 7.
Samples of noise-free and noisy reconstruction images (after 120 updates) for the cold rod phantom for different degrees of multiplexing obtained from (a) scheme 1 (same number of pinholes) and (b) scheme 2 (increasing number of pinholes). Substantial artifacts are observed for noise-free and noisy reconstruction images for both schemes (arrows). The NMSE shown as a function of number of updates for increased degrees of multiplexing for (c) scheme 1 and (d) scheme 2. (e) and (f) The lowest NMSE achieved for different degrees of multiplexing for two schemes. (g) and (h) Corresponding NMSE-to-noise trade-off curves for different degrees of multiplexing for both schemes.
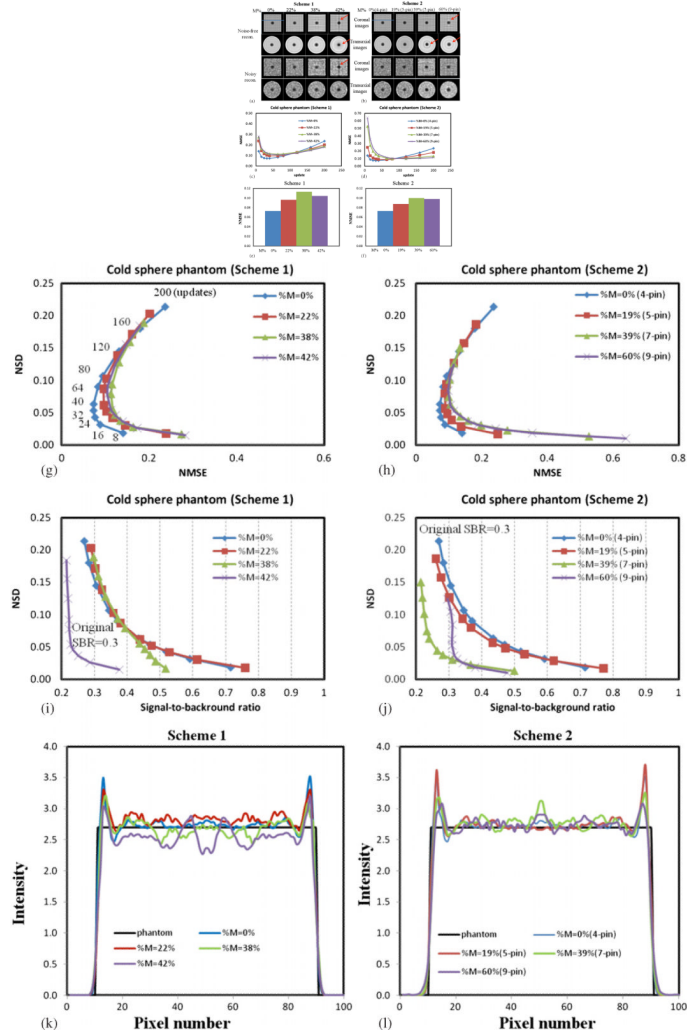
Figure 8.
Samples of noise-free and noisy reconstruction images (coronal and transaxial, 120 updates) for the cold sphere phantom for different degrees of multiplexing obtained from (a) scheme 1 (same pinhole numbers) and (b) scheme 2 (increasing pinhole numbers). Apparent artifacts are observed for both schemes (arrows). The NMSE shown as a function of number of updates for increased degrees of multiplexing for (c) scheme 1 and (d) scheme 2. (e) and (f) The lowest NMSE achieved for different degrees of multiplexing for the two schemes. (g) and (h) Corresponding NMSE-to-noise trade-off curves for different degrees of multiplexing for both schemes. (i) and (j) The SBR-to-noise trade-off for both schemes. (k) and (l) Image profiles drawn along uniform region shown in (a) (blue line).
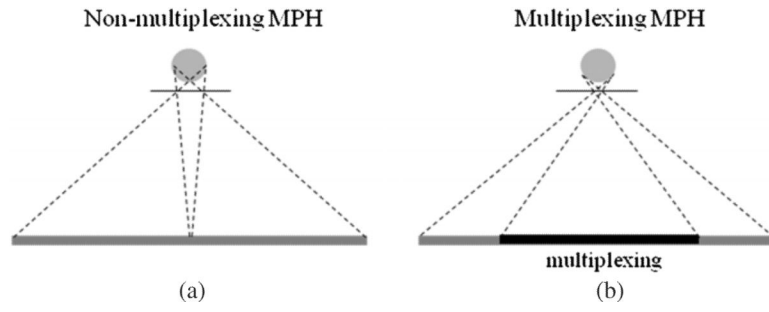
Figure 9.
When compared to (a) non-multiplexing MPH design, (b) multiplexing has the potential to reduce projection truncations for a fixed imaging distance.

Table 1

The design parameters of the MPH collimators used in the study.

Design parameters	Values
Collimator length	7 cm
Pinhole aperture size	1 mm (knife edge)
Acceptance angle	80°
Radius-of-rotation	4 cm
Number of projections	64 over 360°
Intrinsic resolution	1.5 mm
Bin size	1.5 mm
Detector size	12×12 cm

Table 2

Summary of the simulation setup for the two multiplexing schemes.

Multiplexing scheme	Number of pinholes	Phantom	% of multiplexing (projection space)	Note
1	4	Hot rod	0, 14, 32, 40	Same magnification and detection efficiency
		Cold rod	0, 22, 33, 40	
		Cold sphere	0, 22, 38, 42	
2	4, 5, 7, 9	Hot rod	0, 12, 31, 50	Same magnification with altered detection efficiency
		Cold rod	0, 18, 38, 60	
		Cold sphere	0, 19, 39, 60	